Large-mode-area infrared guiding in ultrafast laser written waveguides in Sulfur-based chalcogenide glasses

Ciro d'Amico, Guanghua Cheng, Cyril Mauclair, Johann Troles, Laurent Calvez, Virginie Nazabal, Celine Caillaud, Guillermo Martin, Brahim Arezki, Etienne Lecoarer, et al.

Large-mode-area infrared guiding in ultrafast laser written waveguides in Sulfur-based chalcogenide glasses

C. D'Amico,[1] G. Cheng,[1,2] C. Mauclair,[1] J. Troles,[3] L. Calvez,[3] V. Nazabal,[3] C. Caillaud,[3] G. Martin,[4] B. Arezki,[4] E. LeCoarer,[4] P. Kern,[4] and R. Stoian[1,*]

[1]*Laboratoire Hubert Curien, UMR 5516 CNRS, Université de Lyon, Université Jean Monnet, 42000 St. Etienne, France*

[2]*State Key Laboratory of Transient Optics and Photonics, Xi'an Institute of Optics and Precision Mechanics, CAS, 710119 Xi'an Shaanxi, China*

[3]*Chemical Sciences Institute of Rennes, UMR 6226 CNRS, University of Rennes I, 35042 Rennes, France*

[4] *Institut de Planetologie et d'Astrophysique de Grenoble, UMR 5274 CNRS, Université Joseph Fourier, 38041 Grenoble, France*

razvan.stoian@univ-st-etienne.fr

Abstract: Current demands in astrophotonics impose advancing optical functions in infrared domains within embedded refractive index designs. We demonstrate concepts for large-mode-area guiding in ultrafast laser photowritten waveguides in bulk Sulfur-based chalcogenide glasses. If positive index contrasts are weak in As_2S_3, Ge doping increases the matrix rigidity and allows for high contrast (10^{-3}) positive refractive index changes. Guiding with variable mode diameter and large-mode-area light transport is demonstrated up to 10 μm spectral domain using transverse slit-shaped and evanescently-coupled multicore traces.

OCIS codes: (140.3390) Laser materials processing; (320.2250) Femtosecond phenomena; (230.7370) Waveguides; (130.3120) Integrated optics devices; (160.2750) Glass and other amorphous materials; (130.3060) Infrared.

References and links

1. J. Bland-Hawthorn and P. Kern, "Astrophotonics: a new era for astronomical instruments," Opt. Express **17**, 1880–1884 (2009).
2. J. Bland-Hawthorn, M. Englund, and G. Edvell, "New approach to atmospheric OH suppression using an aperiodic fibre Bragg grating," Opt. Express **12**, 5902–5909 (2004).
3. P. Houizot, C. Boussard-Plédel, A. J. Faber, L. K. Cheng, B. Bureau, P. A. Van Nijnatten, W. L. M. Gielesen, J. Pereira do Carmo, and J. Lucas, "Infrared single mode chalcogenide glass fiber for space," Opt. Express **15**, 12529-12538 (2007).
4. E. le Coarer, S. Blaize, P. Benech, I. Stefanon, A. Morand, G. Léronde, G. Leblond, P. Kern, J. M. Fedeli, and P. Royer, "Wavelength-scale stationary-wave integrated Fourier transform spectrometry," Nat. Phot. **1**, 473-478 (2007).
5. T. A. Birks, B. J. Mangan, A. Díez, J. L. Cruz, and D. F. Murphy, "Photonic lantern spectral filters in multi-core fibre," Opt. Express **20**, 13996-14008 (2012).
6. F. Malbet, P. Kern, I. Schanen-Duport, J. -P. Berger, K. Rousselet-Perraut, and P. Benech, "Integrated optics for astronomical interferometry. I. Concept and astronomical applications," Astron. Astrophys. Suppl. Ser **138**, 135–145 (1999).
7. D. Noordegraaf, P. M. W. Skovgaard, M. D. Nielsen, and J. Bland-Hawthorn, "Efficient multi-mode to single-mode coupling in a photonic lantern," Opt. Express **17**, 1988-1994 (2009).

#207732 - $15.00 USD Received 5 Mar 2014; revised 1 May 2014; accepted 1 May 2014; published 22 May 2014

8. B. J. Eggleton, "Chalcogenide photonics: fabrication, devices and applications Introduction," Opt. Express **18**, 26632–26634 (2010).
9. J. Hu, J. Meyer, K. Richardson, and L. Shah, "Feature issue introduction: mid-IR photonic materials," Opt. Mat. Express **3**, 1571–1575 (2013).
10. V. G. Ta'eed, N. J. Baker, L. Fu, K. Finsterbusch, M. R. E. Lamont, D. J. Moss, H. C. Nguyen, B. J. Eggleton, D. Y. Choi, S. Madden, and B. Luther-Davies, "Ultrafast all-optical chalcogenide glass photonic circuits," Opt. Express **15**, 9205–9221 (2007).
11. A. Zakery and S. Elliott, "Optical properties and applications of chalcogenide glasses: a review," J. Non-Cryst. Solids **330**, 1–12 (2003).
12. J. S. Sanghera and I. D. Aggarwal, "Active and passive chalcogenide glass optical fibers for IR applications: a review," J. Non-Cryst. Solids **256–257**, 462–467 (2008).
13. X. Gai, T. Han, A. Prasad, S. Madden, D.-Y. Choi, R. Wang, D. Bulla, and B. Luther-Davies, "Progress in optical waveguides fabricated from chalcogenide glasses," Opt. Express **18**, 26635–26646 (2010).
14. L. Labadie, G. Martin, N. C. Anheier, B. Arezki, H. A. Qiao, B. Bernacki, and P. Kern, "First fringes with an integrated-optics beam combiner at 10 μm. A new step towards instrument miniaturization for mid-infrared interferometry," Astronomy and Astrophysics **531**, A48, (2011).
15. R. R. Thomson, A. K. Kar, and J. Allington-Smith, "Ultrafast laser inscription: an enabling technology for astrophotonics," Opt. Express **17**, 1963–1969 (2009).
16. N. Cvetojevic, N. Jovanovic, J. Lawrence, M. Withford, and J. Bland-Hawthornn, "Developing arrayed waveguide grating spectrographs for multi-object astronomical spectroscopy," Opt. Lett. **20**, 2062–2072 (2012).
17. N. Jovanovic, P. G. Tuthill, B. Norris, S. Gross, P. Stewart, N. Charles, S. Lacour, M. Ams, J. S. Lawrence, A. Lehmann, C. Niel, J. G. Robertson, G. D. Marshall, M. Ireland, A. Fuerbach, and M. J. Withford, "Starlight demonstration of the Dragonfly instrument: an integrated photonic pupil-remapping interferometer for high-contrast imaging," Mon. Not. R. Astron. Soc. **427**, 806–815 (2012).
18. R. R. Thomson, T. A. Birks, S. G. Leon-Saval, A. K. Kar, and J. Bland-Hawthorn, "Ultrafast laser inscription of an integrated photonic lantern," Opt. Express **19**, 5698–5705 (2011).
19. J. Lucas, "Infrared glasses," Cur. Op. Sol. St. Mat. Sci. **4**, 181–187 (1999).
20. J. A. Savage, "Optical properties of chalcogenide glasses," J. Non-Cryst. Solids **47**, 101-116 (1982).
21. B. Bureau, X. H. Zhang, F. Smektala, J.-L. Adam, J. Troles, H.-li Ma, C. Boussard-Plédel, J. Lucas , P. Lucas , D. Le Coq, M. R. Riley, and J. H. Simmons, "Recent advances in chalcogenide glasses ," J. Non-Cryst. Solids **345–346**, 276–283 (2004).
22. J. S. Sanghera, C. M. Florea, L. B. Shaw, P. Pureza, V.Q. Nguyen, M. Bashkansky, Z. Dutton, and I. D. Aggarwal, "Non-linear properties of chalcogenide glasses and fibers," J. Non-Cryst. Solids **354**, 462–467 (2008).
23. H. Kanbara, S. Fujiwara, K. Tanaka, H. Nasu, and K. Hirao, "Third-order nonlinear optical properties of chalcogenide glasses," Appl. Phys. Lett. **70**, 925–927 (1997).
24. K. S. Bindra, H. T. Bookey, A. K. Kar, B. S. Wherrett, X. Liu, and A. Jha, "Nonlinear optical properties of chalcogenide glasses: Observation of multiphoton absorption," Appl. Phys. Lett. **9**, 1939–1941 (2001).
25. T. Cardinal, K. A. Richardson, H. Shim, A. Schulte, R. Beatty, K. Le Foulgoc, C. Meneghini, J. F. Viens, and A. Villeneuve, "Non-linear optical properties of chalcogenide glasses in the system As-S-Se," J. Non.Cryst Solids **256-257**, 353–360 (1999).
26. G. Boudebs, F. Sanchez, J. Troles, and F. Smektala, "Nonlinear optical properties of chalcogenide glasses: comparison between MachZehnder interferometry and Z-scan techniques," Opt. Commun. **199**, 425-433 (2001).
27. J.-F. Viens, C. Meneghini, A. Villeneuve, T. V. Galstian, E. J. Knystautas, M. A. Duguay, K. A. Richardson, and T. Cardinal, "Fabrication and characterization of integrated optical waveguides in sulfide chalcogenide glasses," J. Lightwave Tech. **17**, 1184–1991 (1999).
28. T. Han, S. Madden, D. Bulla, and B. Luther-Davies, "Low loss Chalcogenide glass waveguides by thermal nanoimprint lithography," Opt. Express **18**, 19286–19291 (2010).
29. K. Tanaka, "Photoexpansion in As_2S_3 glass," Phys. Rev. B **57**, 5163–5167 (1998).
30. K. Tanaka, "Structural phase transitions in chalcogenide glasses," Phys. Rev. B **39**, 1270–1279 (1989).
31. H. Fritzche "Photo-induced fluidity of chalcogenide glasses," Solid State Commun. **99**, 153–155 (1996).
32. V. M. Lyubin, and V. K. Tikhomirov, "Novel photo-induced effects in chalcogenide glasses ," J. Non-Cryst. Solids **135**, 37-48 (1991).
33. J. P. De Neufville, S. C. Moss, and S. R. Ovshinsky, "Photostructural transformations in amorphous As2Se3 and As2S3 films," J. Non-Cryst. Solids **13**, 191-223 (1974).
34. G. Chen, H. Jain, M. Vlcek, S. Khalid, J. Li, D. A. Drabold, and S. R. Elliott, "Observation of light polarization-dependent structural changes in chalcogenide glasses," Appl. Phys. Lett. **82**, 606–608 (2003).
35. H. Jain, S. Krishnaswami, A. C. Miller, P. Krecmer, S. R. Elliott, and M. Vlček, "In situ high-resolution X-ray photoelectron spectroscopy of light-induced changes in As-Se glasses," J. Non-Crys. Solids **274**, 115-123 (2000).
36. O. M. Efimov, L. B. Glebov, K. A. Richardson, E. Van Stryland, T. Cardinal, S. H. Park, M. Couzi, and J. L. Bruneel, "Waveguide writing in chalcogenide glasses by a train of femtosecond laser pulses," Opt. Mater. **17**, 379–386 (2001).
37. C. Meneghini and A. Villeneuve, "As_2S_3 photosensitivity by two-photon absorption: holographic gratings and

#207732 - $15.00 USD Received 5 Mar 2014; revised 1 May 2014; accepted 1 May 2014; published 22 May 2014

self-written channel waveguides," J. Opt. Soc. Am. B **15**, 2946–2950 (1998).
38. A. M. Ljungström and T. M. Monro, "Light-Induced Self-Writing Effects in Bulk Chalcogenide Glass," J. Lightwave Technol. **20**, 78–85 (2002).
39. M. Hughes, W. Yang, and D. Hewak, "Fabrication and characterization of femtosecond laser written waveguides in chalcogenide glass," Appl. Phys. Lett. **90**, 131113 (2007).
40. N. D. Psaila, R. R. Thomson, H. T. Bookey, S. Shen, N. Chiodo, R. Osellame, G. Cerullo, A. Jha, A. K. Kar, "Supercontinuum generation in an ultrafast laser inscribed chalcogenide glass waveguide," Opt. Express **15**, 15776–15781 (2007).
41. O. Caulier, D. Le Coq, L. Calvez, E. Bychkov, and P. Masselin, "Free carrier accumulation during direct laser writing in chalcogenide glass by light filamentation," Opt. Express **19**, 20088–20096 (2011).
42. M. A. Hughes, W. Yang, and D. W. Hewak, "Spectral broadening in femtosecond laser written waveguides in chalcogenide glass," J. Opt. Soc. Am. B **26**, 1370–1378 (2010).
43. S. Juodkazis, T. Kondo, H. Misawa, A. Rode, M. Samoc, and B. Luther-Davies "Photo-structuring of As_2S_3 glass by femtosecond irradiation," Opt. Express **14**, 7751–7756 (2006).
44. A. Ródenas, G. Martin, B. Arezki, N. Psaila, G. Jose, A. Jha, L. Labadie, P. Kern, A. Kar, and R. Thomson, "Three-dimensional mid-infrared photonic circuits in chalcogenide glass," Opt. Lett. **37**, 392–394 (2012).
45. A. Zoubir, M. Richardson, C. Rivero, A. Schulte, C. Lopez, K. Richardson, N. Ho, and R. Vallée, "Direct femtosecond laser writing of waveguides in As_2S_3 thin films," Opt. Lett. **29**, 748-750 (2004).
46. T. Anderson, N. Carlie, L. Petit, J. Hu, A. Agarwal, J. J. Viens, J. Choi, L. C. Kimmerling, K. Richardson, and M. Richardson, "Refractive index modifications in Chalcogenide films induced by sub-bandgap near-IR femtosecond pulses," Paper CThS6 CLEO conference (2007).
47. P. Masselin, D. Le Coq, A. Cuisset, and E. Bychkov, "Spatially resolved Raman analysis of laser induced refractive index variation in chalcogenide glass," Opt. Mat. Express **2**, 1768–1775 (2012).
48. A. Mermillod-Blondin, C. Mauclair, A. Rosenfeld, J. Bonse, I. V. Hertel, E. Audouard, and R. Stoian, "Size correction in ultrafast laser processing of fused silica by temporal pulse shaping," Appl. Phys. Lett. **93**, 021921 (2008).
49. O. Caulier, D. Le Coq, E. Bychkov, and P. Masselin, "Direct laser writing of buried waveguide in As_2S_3 glass using a helical sample translation," Opt. Lett. **38**, 4212–4215 (2013).
50. Y. Cheng, K. Sugioka, K. Midorikawa, M. Masuda, K. Toyoda, M. Kawachi, and K. Shihoyama, "Control of the cross-sectional shape of a hollow microchannel embedded in photostructurable glass by use of a femtosecond laser," Opt. Lett. **28**, 55–57 (2003).
51. G. Cheng, C. D'Amico, X. Liu, and R. Stoian, "Large mode area waveguides with polarization functions by volume ultrafast laser photoinscription of fused silica," Opt. Lett. **38**, 1924–1927 (2013).
52. B. McMillen, B. Zhang, K. P. Chen, A. Benayas, and D. Jaque, "Ultrafast laser fabrication of low-loss waveguides in chalcogenide glass with 0.65 dB/cm loss," Opt. Lett. **37**, 1418–1420 (2012).
53. M. M. Vogel, M. Abdou-Ahmed, A. Voss, and T. Graf, "Very-large-mode-area, single-mode multicore fiber," Opt. Lett. **34**, 2876–2878 (2009).

1. Introduction

Present demands in astrophotonics impose advancing optical functions and accessibility in mid-infrared (MIR) spectral ranges, enhancing as well the efficiency of photon harvesting and transport [1]. This concerns astronomy and space sensing applications, particularly in tracking molecular organic tracers. Miniaturization in dedicated optical instrumentation targets now specifically the fabrication of three-dimensional (3D) photonic circuitries in adapted optical materials with transparency window up to 14 μm.

Photonic developments in the area of multiplexed spectroscopy or for interferometric combination of beams from large telescopes were dominantly based on planar technologies and fibers. These include already a range of functionalities and systems such as waveguide combiners in miniaturized spectrographs and interferometers, broadband Bragg gratings for suppression of unwanted spectral signatures (e.g. OH), or photonic lanterns with phase-controlled modal behaviors [2–7]. The extension to the third dimension in compact geometries allows to address the complexity of the coming generation of astronomical instruments (especially for multi object spectroscopy and stellar interferometry) due to the embedded nature of the technology. Basic optical functions (e.g. light manipulation including wavefront filtering, beam splitting, combination, and reshaping) can be integrated within a unique compact photonic device, and contribute to the development of complex "instruments without bulk optics" with phase and

#207732 - $15.00 USD Received 5 Mar 2014; revised 1 May 2014; accepted 1 May 2014; published 22 May 2014

modal control for astronomy signal collection. Second, 3D geometries allow for further flexibility in the MIR spectral range for photonics-based astronomical instruments. The spectral domains of 3-5 μm and 8-12 μm bear great astrophysical importance as numerous molecular organic tracers (water, CO_2, ozone) can be sensed at these wavelengths. The question of accessibility and fabrication requirements puts forward chalcogenide technology as a promising solution with the challenge of creating performant light transport capabilities [8–14].

For designing optical functions relevant for astrophotonics at arbitrary positions, 3D ultrafast laser modification of transparent materials and refractive index engineering offers already interesting perspectives [15–18]. The localized refractive index changes following laser scan allow to create light control functions inside bulk materials where the embedded nature determines intrinsic phase stability. The associated optical properties can provide throughput and flexibility, contributing to efficient light delivery in complex optical designs. The optical performance is linked to the balance between index contrast, profile, and dimension, thus optimal material response to light interaction is determinant. That implies that the physical interaction and its dimensionality have to be accurately controlled for achieving desired mode transport in MIR.

Chalcogenide glasses (ChGs) represent an important class of materials for MIR applications [19–21] due to their transparency and nonlinear strength [22–26], and are currently employed in guiding, nonlinear switching, continuum generation, amplification, or optical recording. Planar and fiber methods including fiber drawing, embossing, deposition/etching, photolithography, photo-darkening, or ion implantation are already developed and implemented for photonic applications [27, 28]. These materials show equally strong photosensitivity and intrinsic metastability, which marks the reaction to external radiation [29–35]. The structural flexibility allows to tune optical properties by elemental constituents, namely gap and phonon energy, or nonlinearities. These features, coupled to a relatively high two photon absorption at current ultrafast laser radiation wavelengths in the transparency window (in the range of cm/GW) permits the development of volume 3D photoinscription methods. Nonlinear bulk photoinscription techniques were already employed to create waveguiding traces using ultrafast laser radiation [36–42], with the demonstration of 3D feasibility [43, 44]. The induced refractive index change has a nonlinear nature and is determined, depending on glass composition, by molecular, structural, and thermomechanical rearrangements [45–47]. With optical guiding demonstrated at visible and NIR wavelengths, the extension to MIR poses further challenges. Traces photoinscribed by volume direct laser writing are limited in cross-section due to the usually employed tight focusing geometries and in index contrast, and, therefore, the normalized frequency is intrinsically low in MIR, creating delocalized modes and inducing losses.

Here we present concepts of large-mode-area guiding in IR and MIR spectral domains in $As_{40}S_{60}$ (As_2S_3) and $Ge_{15}As_{15}S_{70}$, compatible with large normalized frequencies and low numerical apertures for efficient collection of light up to 10 μm. We firstly show that Ge insertion in As_2S_3 significantly enhances the processing window for positive refractive index changes, by gap engineering. We then indicate that variable mode dimensions particularly attractive for MIR can be realized using slit-shaping and multicore guide bundle designs. Characterization in a large spectral domain shows good guiding properties and moderate chromaticity.

2. Experimental description

An amplified Ti:sapphire ultrafast laser system delivering 800 nm light pulses of 500 mW power at a variable repetition rate of 10–100 kHz and a nominal output pulse duration of 130 fs was employed as irradiation source. The source is equipped with a pulse envelope control unit in time and space domains based on spectral and spatial phase modulation [48]. Exposure doses were controlled by electromechanical shutters. As_2S_3 and $Ge_{15}As_{15}S_{70}$ parallelepipedic samples with transparency cut-off in the 520–580 nm domain were employed, mounted on XYZ

#207732 - $15.00 USD Received 5 Mar 2014; revised 1 May 2014; accepted 1 May 2014; published 22 May 2014

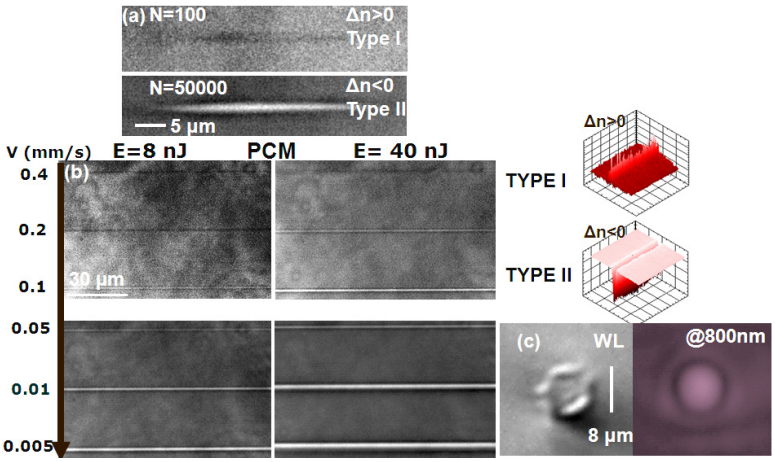

Fig. 1. Ultrafast laser (150 fs) photoinscription results in As_2S_3 glass in terms of PCM phase retardation maps for static and longitudinally scanned conditions. (a) PCM images of static traces at different accumulation doses: N=100 and 20 nJ, and N=50000 and 2 nJ at 100 kHz, illustrating positive and negative index change domains. (b) PCM images of longitudinally scanned photoinscription domains with positive and negative index changes, depending on scan velocity and input energy (10 kHz laser repetition rate). Laser parameters are given on the figure for NA=0.45 focusing. Insert: Refractive index qualitative profiles from Abel inverse transformation of retardation charts. (c) Depressed cladding guide made by partly overlapping type II traces and the corresponding mode at 800 nm. Experimental conditions: 20 nJ per pulse, 100 kHz repetition rate, 0.5 mm/s scan speed.

motion stages that allow translation parallel or perpendicular to the laser propagation axis. The beam was focused inside the target by various focusing optics, including large focal distance microscope objectives (NA=0.42–0.45, effective NAs due to truncation limited to NA=0.4) or aspherical lenses (NA=0.5). Static and longitudinal writing configurations with translation parallel to the laser axis and in the direction of the laser source were used in direct focusing geometries, with power compensation schemes to correct spatial distortions at increasing focusing depths. Slit-shaping techniques with typical slit dimensions of 100 μm and afocal cylindrical telescopes for astigmatic corrections were employed with transverse scans. An Olympus BX 41 positive optical phase-contrast microscope inserted in the irradiation setup was used to image the interaction region in real-time in a side-view geometry. Positive refractive index changes relative to the background matrix are appearing dark on gray background, while white zones indicate negative index variations. The phase contrast microscopy (PCM) was accompanied by white light transillumination imaging (WL). The guiding properties were verified upon injection with IR and MIR light. Laser radiation at 0.8 μm, 3.39 μm in combination with FLIR camera, and a large band black body source spectrally limited by a HgCdTe monopixel detector at 3-11 μm were used. Radiation was injected via 0.2 NA objectives adapted for respective domains (glass or ZnSe) and imaging off-axis $f/1$ parabolas.

3. Results and discussion

3.1. Laser photoinscription

3.1.1. As_2S_3 glass

Laser modification effects in bulk As_2S_3 present several particularities as a function of energy. These are depicted in Figs. 1(a) and 1(b) as PCM images of the retardation charts

#207732 - $15.00 USD Received 5 Mar 2014; revised 1 May 2014; accepted 1 May 2014; published 22 May 2014

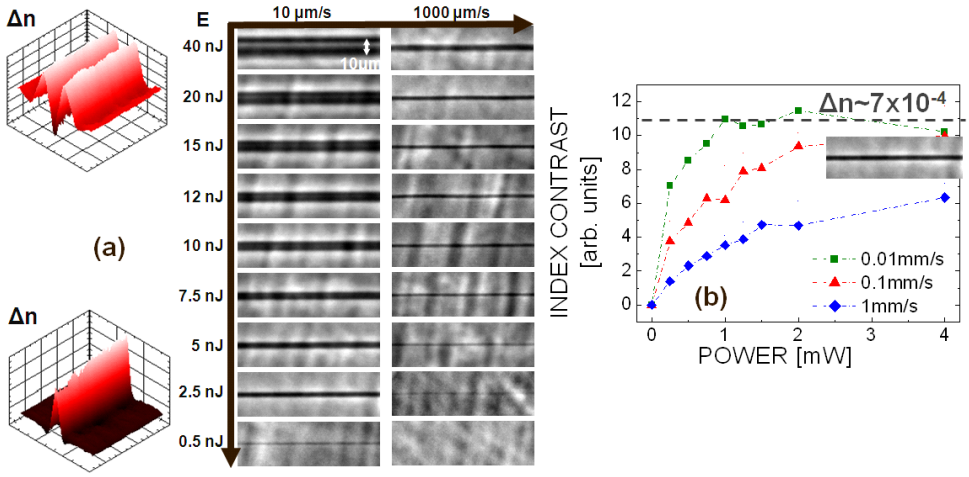

Fig. 2. (a) Ultrafast laser (150 fs) photoinscription results in terms of PCM phase retardation maps in $Ge_{15}As_{15}S_{70}$ glass as a function of the input energy for two different scan velocities. Longitudinal scan geometries are used with NA=0.5 aspheric focusing. Dominantly positive index increase is obtained in the laser-modified regions, with an observable onset of negative changes in the center region at large accumulation doses. The inserts represent characteristic qualitative index change profiles from inverse Abel transform of the retardation maps. (b) Cumulative behavior and dose-dependent index increase as a function of input power and scan velocity, amounting to high index contrast.

($\int_\Delta n(x,y,z)\,dz$) in static and longitudinally scanned conditions, at various energies and scan velocities/exposure doses. The following behavior can be observed for both static and scanned traces. At low accumulation doses and low energies (around the critical self-focusing, i.e. in the nJ domain), ultrafast laser radiation induces a weak ($\leq 10^{-4}$) positive index change, denoted here as type I. This is usually attributed to the formation of homopolar bonds after breaking heteropolar bonding [36, 45]. Interestingly, in the employed energy domain (2-40 nJ), the material response commences with a positive index changes and changes upon accumulation to negative values, suggesting a strong cumulative effect. Negative index changes can be induced at low pulse numbers and high energies. The increase of the accumulation dose determines an apparent heat-driven thermomechanical expansion of the material, leading to a negative index change (type II). This response appears rather confined in cross-section, suggesting that even for typical diffusivities of sulfur-based chalcogenide glasses ($1 \div 3 \times 10^{-7}$ m^2/s), few times lower than that of model fused silica, thermal multipulse accumulation may be only incipient in our conditions, adding on other forms of stress and structural incubation. Index profiles in the different photoinscription regimes are illustrated by the Abel transform on the retardation charts of longitudinally scanned traces [inserts Fig. 1(b)]. Raman analysis has not shown strong spectral variations with respect to the non-modified glass in type I and II cases, except a zone around 220-235 cm^{-1} where usually As–As vibration modes are reported.

As the window of positive index processing is relatively low, this glass is particularly attractive for depressed cladding waveguides [49]. A design method consisting of partially overlapping longitudinal type II traces disposed in cylindrical geometry was used. A WL transillumination image of the resulting depressed cladding guide with the transmitted mode at 800 nm is given in Fig. 1(c). The guiding is found to be lossy (amounting to tens of dB/cm), potentially related to the roughness of the interface and the absence of significant stress accumulation towards the center of the structure.

#207732 - $15.00 USD Received 5 Mar 2014; revised 1 May 2014; accepted 1 May 2014; published 22 May 2014

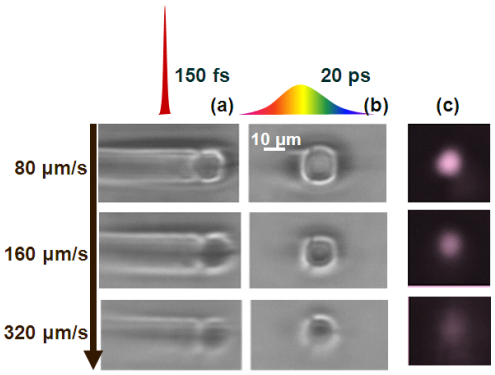

Fig. 3. Transverse slit-shaping photoinscribed traces in $Ge_{15}As_{15}S_{70}$ glass as a function of the pulse duration and accumulation dose (scan speed). Incident power of 30 mW at 100 kHz was delivered via a 100 μm slit and focused by NA=0.42 objective. (a) Ultrafast irradiation: ultrashort pulse irradiation determines extended damage around the core (WL transillumination image). (b) Irradiation results with elongated linearly chirped pulses. Durations of 20 ps can limit the collateral damage and create symmetric core traces. (c) The guided mode at 800 nm is given for the latter case, illustrating examples with decreasing index contrast.

3.1.2. $Ge_{15}As_{15}S_{70}$ glass

The insertion of Ge as a network modifier, leading to a $Ge_{15}As_{15}S_{70}$ composition, has a dramatic effect on the laser processing window. The parameters domain for obtaining positive index contrast is significantly increased and this represents now the dominant material response. The situation is depicted in Fig. 2(a) for a range of input energies and scan velocities. The transformation can be associated with an increasing of the average coordination number of the glass following the insertion of the network modifier, indicative of a more rigid matrix. Adding a fourfold coordinating element such as Ge permits therefore to obtain more stable positive index changes. Moreover, the visible cut-off frequency increases as well, with a spectral displacement from 580 nm for As_2S_3 to 520 nm for $Ge_{15}As_{15}S_{70}$. Consequently, the linear and the nonlinear absorption at 800 nm (the photoinscription wavelength) become weaker in the $Ge_{15}As_{15}S_{70}$ glass than in the As_2S_3 glass and permits stronger, less-heat-accompanied photoinscribed modifications in the material. $Ge_{15}As_{15}S_{70}$ has a refractive index of 2.21 at 800 nm as compared to 2.52 for the As_2S_3, allowing reduced Fresnel losses during photowriting.

Refractive index estimations based on the numerical aperture of the 100 kHz ultrafast laser written longitudinal guides at 800 nm injection suggest a high contrast of up to 10^{-3}. The guide index contrast can be controlled by the incoming energy and deposition rate, building up on a structural accumulation effect. Fig. 2(b) shows the dose dependence of the PCM retardation. The index contrast follows a similar increase with a slightly reduced slope as the dimension of the guide increases somewhat with the dose. We sidenote that further adding of Ge (e.g. $Ge_{20}As_{20}S_{60}$) decreases the processing window for positive index changes, permitting index changes with stronger sensitivity to the laser parameters.

3.2. MIR waveguiding traces

The requirements of single mode guiding in the MIR domain impose constraints on minimal traces diameters (with ranges in the tens of μm) and index contrast (approaching or exceeding 10^{-3}). In response to these limitations we have tested two approaches, namely the slit-shaping method [50] and the evanescently coupled multicore guide bundles [51].

#207732 - $15.00 USD Received 5 Mar 2014; revised 1 May 2014; accepted 1 May 2014; published 22 May 2014

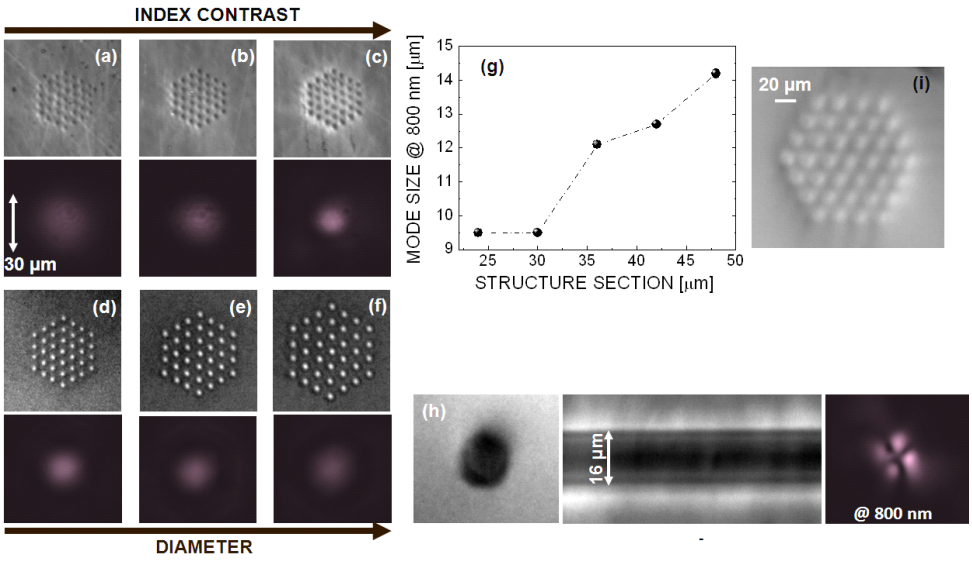

Fig. 4. Multicore waveguiding results in $Ge_{15}As_{15}S_{70}$ glass for ultrashort pulse irradiation. (a,b,c) Multicore cross-sectional profiles in PCM with increasing index contrast and respective guiding behavior at 800 nm. Visible mode confinement appears for higher index contrast. Experimental conditions: (a) 0.4 mW at 0.4 mm/s, (b) 0.4 mW at 0.3 mm/s and (c) 0.8 mW at 0.4 mm/s and 100 kHz via NA=0.42. The transverse size is 30 μm. (d,e,f) Multicore cross-sectional profiles in PCM with increasing intertrace distances and corresponding mode behavior at 800 nm injection. Experimental conditions: 1.8 mW at 1 mm/s and 100 kHz via NA=0.5 aspherical lens. Transverse dimensions (d) 36 μm, (e) 42 μm, (f) 48 μm. (g) Mode dimensions as a function of the multicore spacing at 800 nm. (h) Continuous large section structure obtained by overlapping traces in cross-section and in a side-view PCM perspective. A higher 800 nm mode LP_{21} is obtained. (i) Large section (100 μm) multicore (WL) with individual slit-shaped traces.

3.2.1. Cross-sectional control via slit-shaping and dispersion control of excitation

McMillen et al. [52] have shown recently that slit-shaping techniques can be applied to high index nonlinear materials such as Ga:La:S chalcogenide glasses. We recall that the technique consists in truncating the input beam in one dimension, increasing thus its projected focal size asymmetrically up to the point that it becomes comparable to the confocal distance, realizing a disk-like form that can be transversely scanned. It was shown that despite the presence of spherical aberrations and Kerr-nonlinearities, low-loss (0.65 dB/cm) guiding traces can be obtained with pulse durations around 1 ps. $Ge_{15}As_{15}S_{70}$ has a higher nonlinear susceptibility and ultrashort pulse propagation at higher energies as required in slit-shaping methods is unstable against filamentation and self-focusing. This is becoming apparent in Fig. 3(a) which shows extended damage around the slit-shaped core. Using dispersion engineering we show that linearly chirped 20 ps pulses can restrict the collateral damage and confine the radiation around the slit shaping zone. This is due to a downsize of the Kerr self-focusing and carrier defocusing along the propagation path allowing to deliver the main energy in the interaction region. The result is given in Fig. 3(b) with the behavior of mode guiding at 800 nm shown in Fig. 3(c) for various index contrast. The typical dimensions obtained by this technique are in the range of 10 μm, dependent on the confocal distance of the input objective, however susceptible of nonlinear deformations at low NA/large confocal distances.

#207732 - $15.00 USD Received 5 Mar 2014; revised 1 May 2014; accepted 1 May 2014; published 22 May 2014

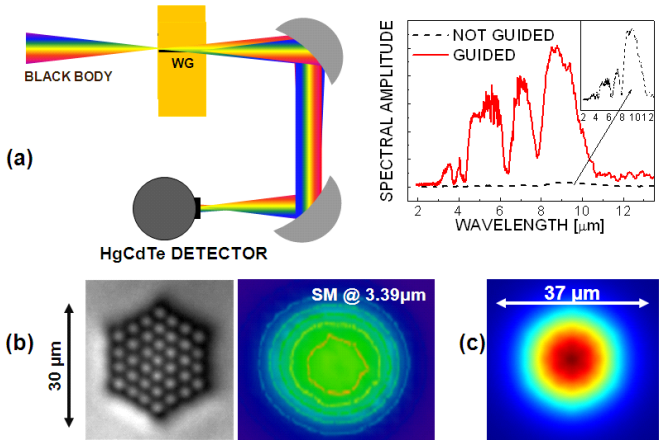

Fig. 5. (a) MIR large band guiding in multicore structures in $Ge_{15}As_{15}S_{70}$ glass (10 mm length). The guided MIR spectrum is compared to the spectrum of the input radiation traversing an equivalent path of non-modified glass (marked as non-guiding). (b) Single mode guiding in a multicore assembly with 5 μm spacing at 3.39 μm injection, detected via a FLIR camera (right). The corresponding structure (also indicated – left) was written at 2.4 mW, 100 kHz input laser conditions via a NA 0.5 aspherical lens at 0.5 mm/s. (c) Finite element analysis for a guided mode at 3.39 μm in a multicore hexagonal structure with 5 μm-spaced, 4 μm thick individual traces of NA=0.08.

3.2.2. Evanescently-coupled multicore guide bundles

Further flexibility in the normalized frequency requires extending the guide cross-section beyond the typical limit of the slit-shaping technique. Evanescently coupled fibers [53] or embedded waveguides [51] were demonstrated to be potential effective solutions for large-mode area transport. Typical hexagonal arrangements with 37 micron-spaced traces were used. The individual traces were longitudinally written on 10 mm lengths, with an automatic energy adjustment as a function of the processing depth to counterbalance spherical aberrations and preserve intensity and dose homogeneity. For typical single trace NA below 0.05, equivalent to index contrasts of up to 5×10^{-4} at 800 nm, the individual modes superpose coherently and create single mode propagation over the bundle cross-section. Higher NA leads to stronger mode localization and favorable conditions for multimode guiding. Results of multicore photoinscription profiles and guiding performances at 800 nm injection are given in Fig. 4 (a)– 4(f), indicating the role of index contrast and structure size. The mode becomes more confined when increasing the index contrasts [Figs. 4 (a), 4(b), and 4(c)] and can be extended with larger trace separation [Figs. 4 (d), 4(e), and 4(f)]. Consequently, the single trace NA can be adjusted for single mode conditions, with losses around 1 dB/cm. The mode size can be increased for a particular index contrast from 200 to 400 μm^2 for 800 nm radiation by trace spacing variations ranging from 3 to 8 μm [Fig. 4 (g)]. Overlapping traces create uniform structures of circular symmetry which behaves multimode at 800 nm, with the onset of the LP_{21} mode [Fig. 4 (h)]. Higher sections (100 μm) with multimode character can be obtained using multicore bundles with slit-shaped individual traces [Fig. 4 (i)].

3.2.3. MIR guiding with large area modes

The extrapolation to larger wavelengths impose constraints on index contrasts and trace diameters. Tests of MIR guiding of multicore structures with index contrasts up or in excess of 10^{-3} are given in Fig. 5. We mention that similar results were obtained for the slit-shaping

#207732 - $15.00 USD Received 5 Mar 2014; revised 1 May 2014; accepted 1 May 2014; published 22 May 2014

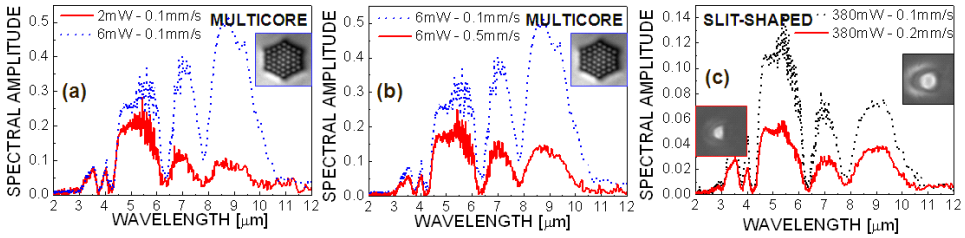

Fig. 6. Spectral dependencies of the laser-induced structures in $Ge_{15}As_{15}S_{70}$ glass at 100 kHz as a function of the index contrast (inserts: representative structures). (a) Power-dependent spectral behavior in multicore traces. Two input powers at 2 mW and 6 mW are compared for similar scan velocities of 0.1 mm/s. Higher contrast leads to better guiding in the large wavelength spectral domain. (b) Dose dependent spectral behavior in multicore traces. Two scan velocities of 0.1 mm/s and 0.5 mm/s are compared at similar input power of 6 mW. Higher contrast leads to better guiding in the large wavelength spectral domain. (c) Dose dependent spectral behavior in slit-shaped traces via two scan velocities (0.1 and 0.2 mm/s) at similar input power of 380 mW. Higher contrast leads to better guide transparency, however overall performances lay below those of the multicore. The observable spectral gaps are related to atmosphere absorption.

structures. Figure 5(a) shows the large-band spectral behavior in the range of 2-12 μm, limited by the material transmission window and detector response. The results indicate high transmittance over the whole source range with peaks related to atmospheric absorption. Spatial mode profiles under coherent light injection were tested at 3.39 μm HeNe laser radiations and show symmetric SM guiding with mode areas up to 1000 μm^2, as indicated in Fig. 5(b), matching the size of the multicore structure. The result is confirmed by 2D finite element analysis (COMSOL Multiphysics) of a long ensemble of multicore traces embedded in a cladding of n=2.155. The simulation, which assumes perfect electric conductor boundary conditions on external boundaries, shows guiding for individual trace NAs above 0.07 (equivalent to a minimal index contrast of 10^{-3}), slightly dependent on trace sections. An example of a calculated mode is given in Fig. 5(c) for a hexagonal structure with 5 μm-spaced, 4 μm traces of NA=0.08; the mode diameter is 37 μm, similar to the measured one. For a range of diameters and intertrace spacings comparable to experiment, NA$\leq$0.07 would lead to leaky modes.

The guiding performances were experimentally analyzed via the cut-back method on multicore guides of several lengths and trace separation of 5 μm. The tests indicate propagation losses in the 1 dB/cm range at 3.39 μm injection. The large band response indicated before shows also expectable chromatic effects with apparent slightly higher attenuation at large wavelengths (above 8 μm) depending on the degree of mode confinement (Fig. 6). However, the chromaticity of the structures is controllable via index contrast, i.e. via the local accumulated radiation dose. This is qualitatively visible in Figs. 6(a) and 6(b) indicating a certain flexibility in chromaticity via the spectrally-dependent evanescently coupling mechanisms, notably a higher large wavelength transparency for higher index contrast. Chromatic effects are less apparent in slit-shaped traces [Fig. 6(c)], with main index contrast effects in the overall guide transparency.

4. Conclusion

In conclusion we have demonstrated highly transparent large-mode-area guiding in Sulfur-based chalcogenide materials, with a particularly high efficiency of photoinduced index change in $Ge_{15}As_{15}S_{70}$. Various irradiation parameters were analyzed exposing composition-

#207732 - $15.00 USD Received 5 Mar 2014; revised 1 May 2014; accepted 1 May 2014; published 22 May 2014

dependent processing windows, indicating cumulative behaviors and possible pulse-envelope control of nonlinearities. Slit-shaped and multicore design are viable solutions for light transport in embedded waveguides.

Acknowledgments

The support of the Agence Nationale de la Recherche, France (project Smart-Lasir 11BS09026) and of the National Natural Science Foundation of China (Project No. 61223007) is gratefully acknowledged. The equipment used at IPAG for wide band and MIR characterization was funded by ANR JC09-507107.

#207732 - $15.00 USD Received 5 Mar 2014; revised 1 May 2014; accepted 1 May 2014; published 22 May 2014